Preprints of the 21st IFAC World Congress (Virtual)
Berlin, Germany, July 12-17, 2020

A model-based fault-detection strategy in DC/AC conversion

A. Pyrkin [*,**] **R. Cisneros** [***] **D.U. Campos-Delgado** [****]
A. Bobtsov [*] **S. Somov** [*]

[*] *ITMO University, 197101 St. Petesburg, Rusia (e-mails: a.pyrkin@gmail.com, bobtsov@mail.ru, s.somov@itmo.ru)*
[**] *Center for Technologies in Robotics and Mechatronics Components, Innopolis University, Innopolis, Russia*
[***] *ITAM, 01080 Mexico City, Mexico (e-mail: rcisneros@itam.mx)*
[****] *UASLP, Facultad de Ciencias, SLP, Mexico (e-mail: ducd@fciencias.uaslp.mx)*

Abstract: An open-circuit fault-detection strategy is here proposed for single-phase DC/AC conversion. The power converter under consideration consists of an H-bridge and a capacitor with parallel resistance and current source in its DC side—these last two stand for the unknown system load and energy injection from renewable resources, respectively. An inductor filter is also included as a coupling element to the AC network. When an open-circuit fault occurs in the H-bridge, the resulting AC output waveform is asymmetric, and induces DC and harmonic components to the network. Hence, by using an additive fault modeling, the fault signature can be expressed by a constant term $f_{\rm dc}$ and a fluctuating signal. The sign of $f_{\rm dc}$ allows to determine the pair of faulty switches in the H-bridge. In this work, an DREM-based identification scheme is proposed to estimate $f_{\rm dc}$. Through the sign of its estimate, it is possible to detect the pair of faulty switches. To assess our approach, simulation results are included.

Keywords: Open-circuit fault-detection, Parameter estimation, DC/AC conversion.

1. INTRODUCTION

Alternative energy sources require a high level of integration into the electrical power grids. For this purpose, DC/AC and AC/AC power converter are used to provide the coupling, synchronization and appropriate power flow to the electrical networks. These power converters employ high-frequency switching to manipulate the energy conversion process. As a result of a constant operation and load transients, the power switches in the DC/AC and AC/AC topologies are facing voltage, current and temperature stresses that could lead to a fault (Salehifar et al., 2015; Yang et al., 2011). After a fault, the DC/AC and AC/AC power converter will not be able to provide a symmetric voltage and current to the electrical network and, consequently, the faulty converter will induce harmonic contamination (Salimian and Iman-Eini, 2017; Jlassi et al., 2015; Mirafzal, 2014). Furthermore, the remaining power switches will suffer more severe voltage and current stresses that could lead to a complete system breakdown. Thus, it is of general interest to detect as quickly as possible a fault condition in power converters, and to subsequently provide a corrective action.

The most common faults scenarios in the power switches are open and short-circuits, that is, short-circuit (SCF) and open-circuit faults (OCF). In OCF the switching devices are unable to close, staying open regardless of their control signal state. On the contrary, in SCF the swithing devices are unable to open. As a matter of fact, by the appropriate protective elements in the converter topology, the SCF will have a similar electrical effect of an OCF. So, this study will focus on OCF. Depending on the pursued strategy, diagnosis and detection of faults can be roughly categorized into signal-based methods, model-based methods, knowledge-based methods, active fault diagnosis methods and hybrid methods which combine different methods. The interested reader is referred to (Gao et al., 2015a,b), where a comprehensive monograph on fault-diagnosis techniques is presented.

This work is placed within the model-based approaches. They stand out because of their fastest detection time compared, for example, to the signal-based schemes, which require more computational time to process the data of the measured signals. Model-based techniques use the mathematical model of the converter to design observers/estimators and construct fault indicator signals—these signals are known as *residuals*. These observers/estimators are designed according to the different methods available in the literature of control systems. Following the sliding mode technique, an observer is derived for OCF diagnosis in multilevel converters in (Mtepele et al., 2019). Fault diagnosis and detection algorithms for motor drive systems are presented in (Jung et al., 2013) based on the model reference adaptive system (MRAS) technique. Meanwhile, in (Salehifar et al., 2015) sliding modes observers are used to detect faults in voltage source inverters (VSI) by the measured and estimated currents in the converter using a cross correlation factor. Finally, proportional-integral observers were employed also to detect faults in VSI and a directional evaluation in the *dq*-

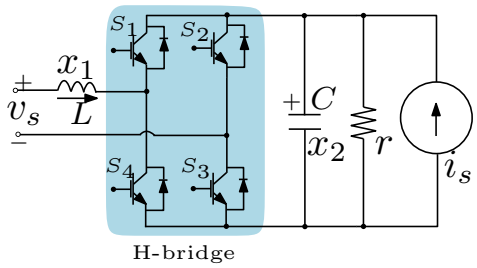

Fig. 1. Power converter under consideration.

frame.

In the current work, we consider the OCF problem in single-phase DC/AC power conversion. The considered power converter consists of a H-bridge, with a parallel array of capacitor, resistor and current source in the DC side, and a coupling inductor filter to the AC network. This is the typical configuration adopted to interface renewable generation units with the AC distribution grid. The current source in the circuit represents the energy generated by the renewable resources and the resistor stands for the system load which is assumed to be unknown.

When OCF takes place in the H-bridge, a pair of switches cannot operate in short circuit. The resulting AC output waveform is asymmetric, and induces DC and harmonic components to the network. Thus, by using an additive fault modeling, the fault signature can be expressed by a constant term f_{dc} and a fluctuating signal. The sign of f_{dc} allows to determine the pair of faulty switches in the H-bridge. In this work, the problem is tackled using a parametric system identification approach that permits to estimate f_{dc} and, therefore, to know its sign. The pursued approach follows from the well-known Dynamic Regressor Extension and Mixing technique (Aranovskiy et al., 2017), also appeared in (Aranovskiy et al., 2016) and successfully implemented in maximum power point tracking problem in photo-voltaic systems (Pyrkin et al., 2017).

The rest of the paper is organized as follows. In Section 2, the system in consideration is introduced and the problem is formulated. In Section 3 we present the procedure which allows to extract the fault indicator signal (residual) from the measurable signals. Section 4 consists of our main result. The proposed estimator is therein presented. The numerical validation of our approach is contained in Section 5. The paper is finalized in Section 6 with our conclusions and future work.

Notation: For $x \in \mathbb{R}^n$ and $Q > 0 \in \mathbb{R}^{n\times n}$, $|x|_Q^2 := x^\top Q x$. For $\hat{x}, x \in \mathbb{R}^n$, we define $\tilde{x} := \hat{x} - x$. For $x(t) \in \mathbb{R}$, we define $x^{(i)} := \frac{d^i}{dt^i}x(t)$, $i \in \mathbb{Z}_{>0}$. When clear from the context, the argument in the functions is omitted.

2. SYSTEM MODELING AND PROBLEM FORMULATION

The average model of the DC/AC power converter of Fig. 1 is

$$M\dot{x} = (Ju - G)x + \begin{bmatrix} v_s \\ i_s \end{bmatrix} \tag{1}$$

where,

$$M = \begin{bmatrix} L & 0 \\ 0 & C \end{bmatrix}, \; G = \begin{bmatrix} 0 & 0 \\ 0 & g \end{bmatrix}, \; J = \begin{bmatrix} 0 & -1 \\ 1 & 0 \end{bmatrix}$$

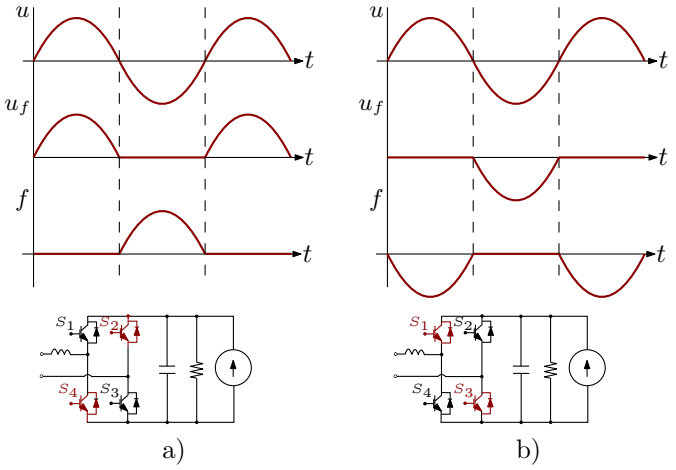

Fig. 2. Control input in nominal condition, faulty control input and fault profiles when: a)an OCF occurs in S_2 and S_4 and b)an OCF occurs in S_1 and S_3.

Also, according to Fig. 1, v_s represents the voltage at the output terminal, $u \in [-1, 1]$ is the duty cycle signal of the H-bridge and the state vector $x^\top = [x_1 \; x_2]$ contains the inductor current and capacitor voltage, respectively. Parameters $g := 1/r$ and L are the unknown load conductance and inductance of the input filter, respectively.

The steady-state of u in nominal conditions is shown in Fig. 2. An OFC occurring in switches S_2 and S_4 leads to the (faulty) input signal u_f of Fig. 2a. Therefore, by using an additive modeling, the fault input signal u_f is expressed as

$$u_f := u + f.$$

A similar analysis can be carried out when a fault occurs in switches S_1 and S_3. The corresponding profiles for u_f and f are depicted Fig. 2b. As can be seen, the fault profile f is a periodic signal in both cases, thus, it can be decomposed as a sum of signals using Fourier series. The oscillatory components will be related to the nominal AC network frequency and its even harmonics. In fact, f can be expressed as

$$f(t) = f_{\text{dc}} + \sum_{i=1}^{n} A_i \sin(\omega_i t + \phi_i) + \varrho_t \tag{2}$$

where f_{dc} is the constant component of the signal and ϱ_t is defined as [1]

$$\varrho_t := \sum_{i=n+1}^{\infty} A_i \sin(\omega_i t + \phi_i), \tag{3}$$

i.e., an infinite sum of frequency components. The parameters A_i, ω_i and ϕ_i correspond to the amplitude, frequency and phase of each harmonic, respectively. Here, it is further assumed that $A_{i+1} < A_i$ for $i \geq 1$. Note that $\varrho_t \in \mathcal{L}_\infty$. Furthermore, by inspection, the constant component f_{dc} is positive when an OFC affects switches S_2 and S_4, and negative otherwise. Then, knowing the sign of f_{dc} permits to detect the pair of faulty switches.

The following assumptions are in order.

A1. L, C, x, v_s and i_s are all known.

[1] Function ϱ_t is a *generic* function of the form presented in (3), namely, a sum of high-frequency harmonics.

A2. The controller dynamics are slower compared to the estimator time constant related to the error convergence.

Parameters L and C of A1 are in fact known as they are selected by the circuit designer. Also, x, v_s and i_s can be measured by sensors. On the other hand, A2 assures that after an occurrence of an OCF, the control-input response time is slow enough so that the parameters of f in (2) can be actually considered constant for a short period of time. This time interval is then sufficiently large for the identification algorithm to give an estimate of $f_{\rm dc}$ and, therefore, to identify the faulty switches. During that interval, the system can be modeled as (Mtepele et al., 2019)

$$M\dot{x} = [Ju_f - G]x + \begin{bmatrix} v_s \\ i_s \end{bmatrix}. \tag{4}$$

2.1 Estimation of g

Being that the load conductance g is unknown, an identification algorithm for g is proposed in the following lemma. The estimated value will be used in the sequel.

Lemma 1. Consider the estimator for g

$$\dot{\hat{g}}_I = -\kappa \hat{g} x_2^2 + \kappa v_s x_1 + \kappa i_s x_2, \quad \kappa > 0 \tag{5a}$$

$$\hat{g} = -\frac{1}{2}\kappa |x|_M^2 + \hat{g}_I \tag{5b}$$

for system (4) and $x_2 \notin \mathcal{L}_2$. Then,

$$\lim_{t\to\infty} \tilde{g}(t) = 0. \tag{6}$$

Proof. The design follows from the I&I methodology (Astolfi et al., 2005). The derivative of the error $\tilde{g} = \hat{g} - g$ is

$$\begin{aligned}\dot{\tilde{g}} =& -\kappa x^\top M \dot{x} + \dot{\hat{g}}_I \\ =& g\kappa x_2^2 - \kappa v_s x_1 - \kappa i_s x_2 + \dot{\hat{g}}_1 \\ =& (\hat{g} - \tilde{g})\kappa x_2^2 - \kappa v_s x_1 - \kappa i_s x_2 + \dot{\hat{g}}_1\end{aligned}$$

Substituting $\dot{\hat{g}}_I$ of (5a) into the last equation results in the error dynamics

$$\dot{\tilde{g}} = -\kappa x_2^2 \tilde{g}$$

whose solution is

$$\tilde{g}(t) = \tilde{g}(0) e^{-\phi(t)}, \ \phi(t) := \kappa \int_0^t x_2^2(s) ds.$$

Therefore, the error is bounded and for $x_2 \notin \mathcal{L}_2$, it converges to zero. Moreover, for $x_2 > 0$, this convergence is exponential. □

3. DERIVATION OF THE FAULT INDICATOR SIGNAL

The fault indicator signal as unmeasurable state may be reconstructed based on available measurements using the technique of nonlinear observer design (Ortega et al., 2015; Pyrkin et al., 2019).

In the following lemma, the fault indicator signal is obtained from the available measurements. This signal is the output of a linear operator driven by the signal $f(t)$, and has the same bias $f_{\rm dc}$ and frequency components ω_i.

Lemma 2. The signal

$$\begin{aligned}y :=& \left[\frac{\alpha}{p+\alpha}\right]\left(-u + \frac{1}{|x|_M^2}\left(L\hat{g}x_1x_2 + Cx_2v_s - Lx_1i_s\right)\right) \\ &- \left[\frac{\alpha p}{p+\alpha}\right]\left(\sqrt{LC}\arctan\left(\sqrt{\frac{L}{C}}\frac{x_1}{x_2}\right)\right),\end{aligned} \tag{7}$$

where $p := \frac{d}{dt}$ is the differentiation operator and $\alpha > 0$ is a constant, has the form of the multisine function

$$y(t) = f_{\rm dc} + \sum_{i=1}^{n} \bar{A}_i \sin(\omega_i t + \bar{\phi}_i) + \varrho_t + \varepsilon_t. \tag{8}$$

for some constants $\bar{A}_i$ and $\bar{\phi}_i$.

Proof. Pre-multiplying (4) by $-x^\top MJ$ yields

$$\begin{aligned}LC(\dot{x}_2x_1 - \dot{x}_1x_2) =& |x|_M^2(u+f) \\ &- [Lgx_1x_2 + Cv_sx_2 - Li_sx_1].\end{aligned} \tag{9}$$

Notice that division by $|x|_M^2$ is allowed since $x_2 > 0$ by assumption. Dividing (9) by $|x|_M^2$ results in

$$\begin{aligned}\frac{LC}{|x|_M^2}(\dot{x}_2x_1 - \dot{x}_1x_2) = u + f - \frac{1}{|x|_M^2}[Lgx_1x_2 \\ + Cv_sx_2 - Li_sx_1].\end{aligned} \tag{10}$$

Notice that

$$\begin{aligned}\frac{LC}{|x|_M^2}(\dot{x}_2x_1 - \dot{x}_1x_2) &= -\sqrt{LC}\sqrt{\frac{L}{C}}\frac{C(\dot{x}_1x_2 - \dot{x}_2x_1)}{Lx_1^2 + Cx_2^2} \\ &= -\sqrt{LC}\frac{1}{1 + \frac{Lx_1^2}{Cx_2^2}}\frac{\dot{x}_1x_2 - \dot{x}_2x_1}{x_2^2}\sqrt{\frac{L}{C}} \\ &= -\sqrt{LC}\frac{1}{1 + \frac{Lx_1^2}{Cx_2^2}}\frac{d}{dt}\left(\sqrt{\frac{L}{C}}\frac{x_1}{x_2}\right) \\ &= -\sqrt{LC}\frac{d}{dt}\left\{\arctan\left(\sqrt{\frac{L}{C}}\frac{x_1}{x_2}\right)\right\}.\end{aligned} \tag{11}$$

From (11), equation (10) is equivalent to

$$\begin{aligned}-\sqrt{LC}\frac{d}{dt}\left\{\arctan\left(\sqrt{\frac{L}{C}}\frac{x_1}{x_2}\right)\right\} = u + f - \frac{1}{|x|_M^2}(Lgx_1x_2 \\ + Cv_sx_2 - Li_sx_1).\end{aligned}$$

After replacing g by $\hat{g} - \tilde{g}$, we get

$$\begin{aligned}f + \frac{L}{|x|_M^2}x_1x_2\tilde{g}v =& -u + \frac{1}{|x|_M^2}(L\hat{g}x_1x_2 + Cv_sx_2 - Li_sx_1) \\ &- \sqrt{LC}\frac{d}{dt}\left\{\arctan\left(\sqrt{\frac{L}{C}}\frac{x_1}{x_2}\right)\right\}.\end{aligned} \tag{12}$$

Processing both sides of (12) through the filter $\frac{\alpha}{p+\alpha}$ with some $\alpha > 0$ yields

$$\begin{aligned}y :=& \left[\frac{\alpha}{p+\alpha}\right]\left(f + \frac{Lx_1x_2\tilde{g}}{|x|_M^2}\right) \\ =& \left[\frac{\alpha}{p+\alpha}\right]\left(-u + \frac{1}{|x|_M^2}(L\hat{g}x_1x_2 + Cv_sx_2 - Lx_1i_s)\right) \\ &- \left[\frac{\alpha p}{p+\alpha}\right]\left(\sqrt{LC}\arctan\left(\sqrt{\frac{L}{C}}\frac{x_1}{x_2}\right)\right).\end{aligned} \tag{13}$$

Notice the following bound

$$\frac{|Lx_1x_2\tilde{g}|}{|x|_M^2} = \frac{1}{C|x|_M^2}|LCx_1x_2||\tilde{g}| \leq \frac{1}{2C}|\tilde{g}|. \quad (14)$$

where Young's inequality and (6) have been used to obtain the last inequality. Hence, the signal y defined in (7) has a form (8). The vanishing term ε_t is due to (14) and the exponentially decaying function resulting from filtering [2]. This completes the proof. □

4. MAIN RESULT

In this section we show how to estimate the parameter f_{dc} of signal (7) which has the form presented in (8).

4.1 Bias Parameterisation

By considering an auxiliary problem, first assume that the signal.

$$y_0(t) := f_{\text{dc}} + \sum_{i=1}^{n} \bar{A}_i \sin(\omega_i t + \bar{\phi}_i) \quad (15)$$

is available for measurement, where all parameters σ, $\bar{A}_i$, ω_i, $\bar{\phi}_i$ are unknown. The goal is to estimate parameter f_{dc}:

$$\lim_{t\to\infty} (f_{\text{dc}} - \hat{f}_{\text{dc}}(t)) = 0. \quad (16)$$

where $\hat{f}_{\text{dc}}$ is an estimate of the true bias f_{dc}.

It is well-known (see, for example, Pyrkin et al. (2015)) that the following relation holds

$$p(p^2+\omega_1^2)(p^2+\omega_2^2)\cdots(p^2+\omega_n^2)y_0 = 0.$$

Introduce a linear filter

$$\xi = \frac{\lambda^{2n+1}}{(p+\lambda)^{2n+1}}\, y_0, \quad \lambda > 0. \quad (17)$$

and invoke the following Lemma.

Lemma 3. (Pyrkin et al. (2015)). The following relation holds for the filter (17) and the input (15)

$$\xi^{(2n+1)} = m^\top(t)\Theta + \varepsilon_t \quad (18)$$

where $m^\top = [\xi^{(2n-1)} \ \dots \ \xi^{(3)} \ \xi^{(1)}]$ is the regressor composed of the functions $\xi^{(j)}(t)$ which are the time derivatives of the filter's output in (17), that is,

$$\xi^{(j)} = \frac{\lambda^{2n+1}p^j}{(p+\lambda)^{2n+1}}\, y_0,$$

and $\Theta^\top := [\theta_1 \ \dots \ \theta_{k-1} \ \theta_k]$ is a vector of parameters depending on the frequencies

$$\begin{cases} \theta_1 &= -\omega_1^2 - \omega_2^2 - \cdots - \omega_n^2, \\ \theta_2 &= -\omega_1^2\omega_2^2 - \omega_1^2\omega_3^2 - \cdots - \omega_{n-1}^2\omega_n^2, \\ &\vdots \\ \theta_n &= -\omega_1^2\omega_2^2\ldots\omega_n^2. \end{cases}$$

and ε_t is an exponentially decaying term.

Proof of Lemma 3 may be found in (Pyrkin et al. (2015)).

Departing from the previous lemma, we present the relation between states of the filter ξ and the bias f_{dc}.

[2] As consequence of the filter's initial condition, additive exponentially decaying terms appear in the filtered signal. As analyzed in (Aranovskiy et al., 2017, 2015), a function $\varepsilon_t \in \mathcal{L}_1$ does not compromise the convergence of the estimators to be presented.

Corollary 1. The following relation holds for the filter (17) and the input (15)

$$f_{\text{dc}} = \xi - \frac{1}{\theta_n}(\xi^{(2n)} - \theta_1\xi^{(2n-2)} - \theta_2\xi^{(2n-4)} - \cdots - \theta_{n-1}\xi^{(2)}) + \varepsilon_t. \quad (19)$$

Proof. Indeed, applying Lemma 3 to the auxiliary signal

$$\xi_0 := \xi - f_{\text{dc}},$$

which is a multisine function of time with zero offset, it is easy to show the next equation

$$\xi_0^{(2n)} = l^\top(t)\Theta + \varepsilon_t, \quad (20)$$

where Θ is defined in Lemma 3 and

$$l^\top = [\xi_0^{(2n-2)} \ \dots \ \xi_0^{(2)} \ \xi_0].$$

Since $\xi_0^{(k)} = \xi^{(k)}$ for all $k > 1$, the equation ξ_{2n} may be rewritten as

$$\xi^{(2n)} = \theta_1\xi^{(2n-2)} + \theta_2\xi^{(2n-4)} + \cdots + \theta_{n-1}\xi^{(2)} + \theta_n(\xi - f_{\text{dc}}) + \varepsilon_t, \quad (21)$$

from which (19) is obtained.

4.2 Estimation of θ

The expression for f_{dc} in (19) depends on values θ_i, which are unkown. It is possible, however, to obtain those values from the linear regressor equation (18). To the best of our knowledge, the most effective approach is well-known DREM technique (Aranovskiy et al. (2017)).

Lemma 4. Consider the estimator $\hat{\Theta}^\top := [\hat{\theta}_1 \ \dots \ \hat{\theta}_{k-1} \ \hat{\theta}_k]$,

$$\dot{\hat{\theta}}_i = \gamma_i\Delta(Y_i - \Delta\hat{\theta}_i), \quad (22)$$

for $\gamma_i > 0$, with $\Delta := \det\{M_e\}$,

$$Y := \operatorname{adj}\{M_e\}\begin{bmatrix} \xi^{(2n+1)} \\ H_1(p)\xi^{(2n+1)} \\ \vdots \\ H_{n-1}(p)\xi^{(2n+1)} \end{bmatrix}, \ M_e := \begin{bmatrix} m^\top \\ H_1(p)m^\top \\ \vdots \\ H_{n-1}(p)m^\top \end{bmatrix}, \quad (23)$$

and linear operators $H_i(p)$ which stand for time delays or linear filters. Then,

$$\lim_{t\to\infty} \tilde{\theta}_i(t) = 0 \iff \Delta \notin \mathcal{L}_2, \quad (24)$$

where $\tilde{\theta}_i$ are elements of the time-varying vector of estimation errors $\tilde{\Theta} := \Theta - \hat{\Theta}$.

Proof. It follows *mutatis mutandi* from (Aranovskiy et al. (2017)).

4.3 Estimation of f_{dc}

Now, the contribution of this work is enunciated by the next proposition.

Proposition 1. Consider the adaptive estimator

$$\hat{f}_{\text{dc}} = \bar{\xi} - \frac{1}{\hat{\theta}_n}\left(\bar{\xi}^{(2n)} - \hat{\theta}_1\bar{\xi}^{(2n-2)} - \cdots - \hat{\theta}_n\bar{\xi}^{(2)}\right), \quad (25)$$

where $\bar{\xi}$ is the output of the LTI filter

$$\bar{\xi} = \frac{\lambda^{2n+1}}{(p+\lambda)^{2n+1}}\, y, \quad (26)$$

driven by the signal y, defined in (7), estimates $\hat{\theta}$ is obtain using DREM procedure described in Lemma 4

$$\dot{\hat{\theta}}_i = \gamma_i \Delta (Y_i - \Delta \hat{\theta}_i), \tag{27}$$

for $\gamma_i > 0$, with $\Delta := \det\{M_e\}$,

$$Y := \operatorname{adj}\{M_e\} \begin{bmatrix} \bar{\xi}^{(2n+1)} \\ H_1(p)\bar{\xi}^{(2n+1)} \\ \vdots \\ H_{n-1}(p)\bar{\xi}^{(2n+1)} \end{bmatrix}, \; M_e := \begin{bmatrix} \bar{m}^\top \\ H_1(p)\bar{m}^\top \\ \vdots \\ H_{n-1}(p)\bar{m}^\top \end{bmatrix},$$

and $\hat{\theta}_i \neq 0$, $\bar{m}^\top = [\bar{\xi}^{(2n-1)} \;\; \dots \;\; \bar{\xi}^{(3)} \;\; \bar{\xi}^{(1)}]$. Then,

(i) $\lim_{t\to\infty} \tilde{f}_{\mathrm{dc}}(t) = 0$, if $\varrho_t = 0$;

(ii) $\limsup_{t\to\infty} |\tilde{f}_{\mathrm{dc}}(t)| \leq C_\varrho$, if $|\varrho_t| \leq C_0$, where the constant C_ϱ depends on the upper bound C_0 of the term ϱ_t.

Proof. Note at the beginning that

$$\begin{aligned} \bar{\xi} &= \frac{\lambda^{2n+1}}{(p+\lambda)^{2n+1}} (y_0 + \varrho_t + \varepsilon_t) \\ &= \xi + \frac{\lambda^{2n+1}}{(p+\lambda)^{2n+1}} (\varrho_t + \varepsilon_t) \\ &= \xi + \varrho_t + \varepsilon_t, \end{aligned} \tag{28}$$

where ϱ_t and ε_t are two generic signals representing the sum of harmonics of small amplitudes and exponentially decaying term. The same property can be concluded for the derivative of $\bar{\xi}$ and ξ.

Therefore, the error $\tilde{f}_{\mathrm{dc}}$ may be described straightforwardly but lengthy as an analytic function of the form

$$\tilde{f}_{\mathrm{dc}} = \mathcal{F}(\|\tilde{\Theta}\|, \varrho_t, \varepsilon_t), \tag{29}$$

which explicitly depends on $\tilde{\Theta}$, disturbance term ϱ_t, and decaying function of time ε_t. Moreover, $\mathcal{F}(0,0,0) = 0$.

The claim (i) follows immediately from Corollary 1 and Lemma 4 since $\tilde{\Theta}$ exponentially converges to 0.

If ϱ_t is not 0, then $\tilde{\Theta}$ converges to a bounded set $\mathcal{Q}$ depending on the upper bound C_0 which is a straightforward result (see, e.g. Bobtsov et al. (2012); Pyrkin et al. (2011)). Then, a constant of the form

$$C_\varrho := \mathcal{F}(\|\mathcal{Q}\|, C_0, 0)$$

which is smaller with decreasing the upper bound C_0 of the disturbance term ϱ_t. □

Remark 1. Equation (18) is a linear regression plus a perturbation term ϱ_t, consisting of high frequency harmonics. If $\varrho_t = 0$, the identification algorithm to be proposed eventually converge to the parameter value. Otherwise, an approximate of Θ can be obtained. Because the amplitudes of the harmonics decrease as their frequencies increase, a good estimate will be obtained by considering a sufficiently large number n of harmonics in (2). We underscore the fact that the sign of f_{dc}, and *not* its actual value, is sufficient to detect the faulty switches.

Remark 2. It is worth mentioning that zero-crossings of $\hat{\theta}_n$ make (25) be indefinite in the instants of time when they occur. This division by zero can be avoided when implementing. Besides, they do not affect the convergence of $\hat{f}_{\mathrm{dc}}$ in the large.

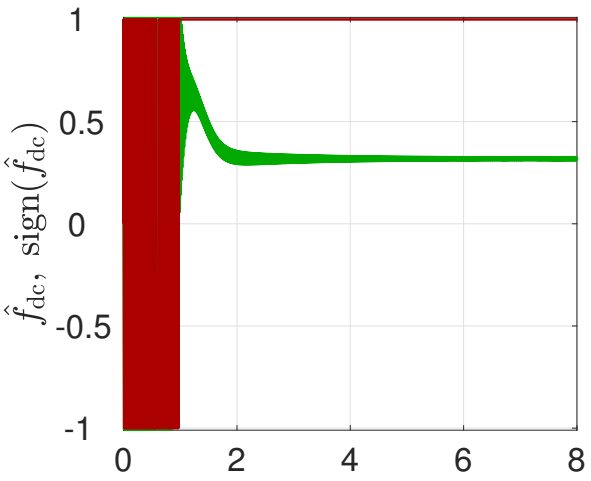

Fig. 3. Fault occurrence in S_2 and S_4: $\hat{f}_{\mathrm{dc}}$, sign($\hat{f}_{\mathrm{dc}}$)

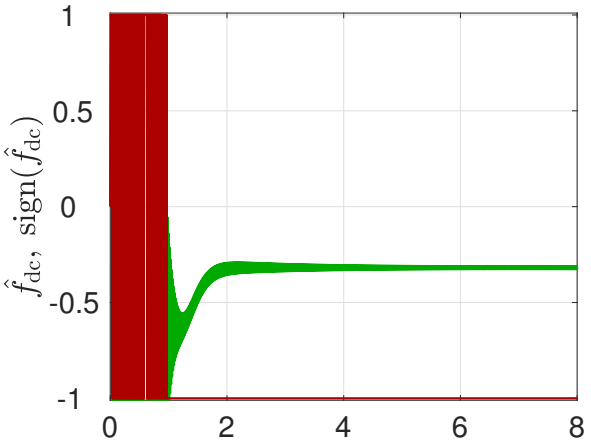

Fig. 4. Fault occurrence in S_1 and S_3: $\hat{f}_{\mathrm{dc}}$, sign($\hat{f}_{\mathrm{dc}}$).

5. SIMULATION RESULTS

The estimator has been numerically validated. For this simulation, we consider a control input $u = \sin 2\pi f_0 t$. The chosen estimator gains are $\alpha = 10$ and $\lambda = 10$—see (7) and (26). We assume two frequencies in the estimator design, that is, $n = 2$. The results are depicted in Fig. 3 and 4. Results for the fault profile in Fig. 2a are shown in Fig. 3. As can be seen, the estimate $\hat{f}_{\mathrm{dc}}$ stays bounded as expected. The signal sign(f_{dc}) has a transitory time-pattern during the initial part of the simulation, and subsequently, it takes the constant value of one, determining the pair of damaged switches (S_2 and S_4). Results for the fault profile in Fig. 2b are shown in Fig. 4. The signal sign(f_{dc}) exhibits a transitory but it finally settles down at -1, thus, detecting the faulty switches S_1 and S_3.

6. CONCLUSIONS & FUTURE WORK

In this work, a model-based strategy for open-circuit fault detection and isolation is proposed. The problem is addressed by utilizing parametric identification techniques to isolate the origin of the fault. The presented scheme is derived from DREM technique.

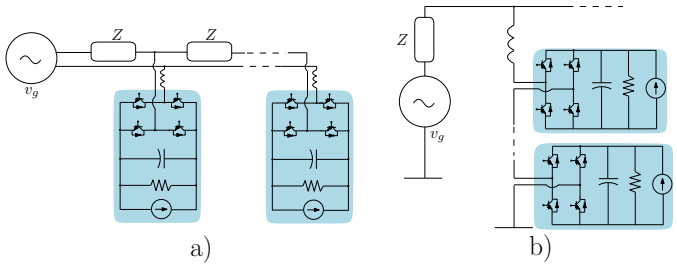

Fig. 5. Fault-detection in: a) Cascade H-Bridge (CHB) and b) Radial topologies.

Our future work has the following three directions.

1. To carry out the experimental implementation of the approach.
2. To incorporate the proposed algorithm to a controller and endow it with fault-tolerant properties. With this purpose, the controllability of the faulty system needs to be analyzed. It is clear that after a fault occurrence, some control degrees of freedom are lost and, as consequence of that, the closed-loop system may no longer accomplish its control task. However, if this is the case, the controller may still maintain the stability of the system despite the fault.
3. To derive a fault-detection strategies, using identification algorithms, for multiconverter connection scenarios. Two scenarios are intended to be analyzed: the radial and cascade topologies—see Fig. 5.

7. ACKNOWLEDGEMENTS

The work was written with the support of the Ministry of Science and Higher Education of the Russian Federation, agreement No. 074-11-2018-029, 13.07.2018, “Creation of high-tech production of robotic flaw detectors for monitoring hard-to-reach welded joints and metal structures of hazardous production facilities in industry, energy and housing”.

REFERENCES

Aranovskiy, S., Bobtsov, A., Ortega, R., and Pyrkin, A. (2017). Performance enhancement of parameter estimators via dynamic regressor extension and mixing. *IEEE Transactions on Automatic Control*, 62(7).

Aranovskiy, S., Bobtsov, A., Pyrkin, A., Ortega, R., and Chaillet, A. (2015). Flux and position observer of permanent magnet synchronous motors with relaxed persistency of excitation conditions. *IFAC-PapersOnLine*, 48(11), 301 – 306. Conference on Modelling, Identification and Control of Nonlinear Systems.

Aranovskiy, S., Bobtsov, A., Ortega, R., and Pyrkin, A. (2016). Improved transients in multiple frequencies estimation via dynamic regressor extension and mixing. *IFAC-PapersOnLine*, 49(13), 99–104.

Astolfi, A., Karagiannis, D., and Ortega, R. (2005). *Nonlinear and Adaptive Control with Applications*. Springer.

Bobtsov, A.A., Efimov, D., Pyrkin, A.A., and Zolghadri, A. (2012). Switched algorithm for frequency estimation with noise rejection. *IEEE transactions on automatic control*, 57(9), 2400–2404.

Gao, Z., Cecatti, C., and Ding, S.X. (2015a). A survey of fault diagnosis and fault-tolerant techniques—part I: fault diagnosis with model-based and signal-based approaches. *IEEE Transactions on Industrial Electronics*, 62(6), 3757–3767.

Gao, Z., Cecatti, C., and Ding, S.X. (2015b). A survey of fault diagnosis and fault-tolerant techniques—part II: fault diagnosis with knowledge-based and hybrid/active approaches. *IEEE Transactions on Industrial Electronics*, 62(6), 3757–3767.

Jlassi, I., Estima, J.O., El-Khil, K., Bellaaj, N.M., and Marques, A.J. (2015). Multiple open-circuit faults diagnosis in back-to-back converters of pmsg drives for wind turbine systems. *IEEE Transactions on Power Electronics*, 30(5), 2689–2702.

Jung, S., Park, J., Kim, H., Cho, K., and Youn, M. (2013). An MRAS-based diagnosis of open-circuit fault in PWM voltage-source inverters for PM synchronous motor drive systems. *IEEE Transactions on Power Electronics*, 28(5), 2514–2526.

Mirafzal, B. (2014). Survey of fault-tolerance techniques for three-phase voltage source inverters. *IEEE Transactions on Industrial Electronics*, 61(10), 5192–5202.

Mtepele, K., Campos-Delgado, D., A.A., V.F., and Pecina, J. (2019). Model-based strategy for open-circuit faults diagnosis in n-level CHB multilevel converters. *IET Power Electronics*, 12(14), 648–655.

Ortega, R., Bobtsov, A., Pyrkin, A., and Aranovskiy, S. (2015). A parameter estimation approach to state observation of nonlinear systems. *Systems & Control Letters*, 85, 84–94.

Pyrkin, A., Bobtsov, A., Ortega, R., Vedyakov, A., and Aranovskiy, S. (2019). Adaptive state observers using dynamic regressor extension and mixing. *Systems & Control Letters*, 133, 104519.

Pyrkin, A., Mancilla-David, F., Ortega, R., Bobtsov, A., and Aranovskiy, S. (2017). Identification of photovoltaic arrays' maximum power extraction point via dynamic regressor extension and mixing. *International Journal of Adaptive Control and Signal Processing*, 31(9), 1337–1349.

Pyrkin, A.A., Bobtsov, A.A., Efimov, D., and Zolghadri, A. (2011). Frequency estimation for periodical signal with noise in finite time. In *2011 50th IEEE Conference on Decision and Control and European Control Conference*, 3646–3651. IEEE.

Pyrkin, A.A., Bobtsov, A.A., Vedyakov, A.A., and Kolyubin, S.A. (2015). Estimation of polyharmonic signal parameters. *Automation and remote control*, 76(8), 1400–1416.

Salehifar, M., Arashloo, R.S., Moreno-Eguilaz, M., Sala, V., and Romeral, L. (2015). Observer-based open transistor fault diagnosis and fault-tolerant control of five-phase permanent magnet motor drive for application in electric vehicles. *IET Power Electronics*, 8, 76–87.

Salimian, H. and Iman-Eini, H. (2017). Fault-tolerant operation of three-phase cascaded H-bridge converters using an auxiliary module. *IEEE Transactions on Industrial Electronics*, 64(2), 1018–1027.

Yang, S., Bryant, A., Mawby, P., Xiang, D., Ran, L., and Tavner, P. (2011). An industry-based survey of reliability in power electronic converters. *IEEE Transactions on Industry Applications*, 47(3), 1441–1451.